Original Article

DOI: 10.5582/irdr.2023.01050

The novel role of IFITM1–3 in myogenic differentiation of C2C12 cells

Yongtao Zhang, Yanqin Lu*, Xianxian Li, Shanshan Zhang, Pengchao Liu, Xiaoyang Hao, Jinxiang Han*

Key Laboratory for Biotech Drugs of the National Health Commission, Key Laboratory for Rare & Uncommon Diseases of Shandong Province, Biomedical Science College & Shandong Medicinal Biotechnology Centre, Shandong First Medical University & Shandong Academy of Medical Sciences, Ji'nan, Shandong, China.

SUMMARY Interferon-induced transmembrane proteins (IFITMs 1, 2, and 3) play a critical role in preventing pathogen infection in vertebrates. They are also involved in the occurrence and prognosis of cancer. Myogenesis is a complex process regulated by several factors. This study disclosed that Ifitm1–3 were upregulated in the process of myogenic differentiation of C2C12 myoblasts on days 3, 5, and 7. This positively correlated with the expression of differentiation factors MyoD, myogenin, Mrf5, and desmin. Furthermore, knockdown of Ifitm1–3 by their individual siRNAs inhibited myogenesis of C2C12 myoblasts, with relative downregulation of MyoD, myogenin, Mrf5, and desmin. Subsequently, myotube formation and fusion percentage decreased. Co-immunoprecipitation combined with LC-MS/MS analysis uncovered the interaction proteins of IFITM1 and IFITM3 in C2C12 myoblasts. A total of 84 overlapped interaction proteins of IFITM1 and IFITM3 were identified, and one of the clusters was engaged in cytoskeletal and sarcomere proteins, including desmin, myosin, actin, vimentin, nestin, ankycorbin, and nucleolin. Hence, we hypothesize that these interacting proteins may function as scaffolds for IFITM1–3, possibly through the interaction protein desmin to initiate further interaction with other proteins to participate in myogenesis; however, the molecular mechanisms remain unclear. Our study may contribute to the development of novel therapeutics for myopathic diseases.

Keywords IFITM1, IFITM3, myogenesis, desmin, sarcomere

1. Introduction

The interferon-inducible transmembrane proteins (IFITMs) belong to the small interferon-stimulated family with molecular mass ranging from 10 to 20 kDa (*1*). The members of this family include IFITM1, IFITM2, IFITM3, IFITM5, and IFITM10 in *Homo sapiens*, and IFITM1, IFITM2, IFITM3, IFITM5, IFITM6, and IFITM10 in mice (*1,2*). IFITM expression can be regulated dependently or independently of interferon signaling (*3-5*).

IFITM1–3 play a synergistic role in antiviral defense, and they are key participants in antiviral immunity (*6-9*). Their expression is upregulated by interferons and other cytokines. When expressed on the cell membrane, they can limit virus–cell membrane fusion, thereby preventing virus entry into the cytoplasm (*10*). IFITM1–3 also suppress viral protein synthesis or viral replication, leading to the reduced production of infectious virions or the lower infectivity of offspring virions (*1,11-13*). IFITM1–3 are also responsible for germ cell homing and maturation during embryonic development (*14,15*). They inhibit placental syncytiotrophoblast fusion (*16-18*). The expression of IFITM5 gradually increases with the differentiation of osteoblasts, and it is an important positive regulator in osteogenic differentiation (*19,20*). *IFITM5* gene mutations lead to type V osteogenesis imperfecta (*21,22*). Low expression of IFITM10 has been reported in re-set positive patients with SARS-CoV-2 infection, and IFITM10 expression level positively correlates with the expression levels of CD69, CD44, NKp30, and granzyme B (*23*). Recently, IFITMs have been implicated in cancer cell progression *via* different pathways (*24-32*).

The process of myogenic differentiation includes the activation, proliferation, and differentiation of resting satellite cells into myoblasts, which fuse to form myotubes, and ultimately mature into muscle fibers that

contain cytoskeletal proteins actin, myosin, desmin, and vimentin, and differentiation factors MyoD, mrf5, MRF4, and myogenin (*33-36*). In this study, we explored the expression of IFITM1–3 in the process of myogenesis and their interaction proteins in myoblasts.

2. Materials and Methods

2.1. Cell culture and myogenic differentiation of C2C12

C2C12 (ATCC) cells were cultured in high-glucose Dulbecco's modified Eagle medium (DMEM) (Lonza, Switzerland) supplemented with 10% (v/v) fetal bovine serum (Gibco, America), 2 mM glutamine (Gibco, USA), 100 U/mL penicillin, and 100 μg/mL streptomycin (Gibco, USA) (growth medium). Cells were maintained at 37°C in a humidified atmosphere containing 5% CO_2 and 95% air. To induce myogenic differentiation, C2C12 cells were grown to 70–80% confluence, with 5×10^4 cells seeded in six-well plates, and then the media were switched to low serum differentiation media (Gibco, USA) (DMEM supplemented with 5% (v/v) horse serum (Gibco, USA) and penicillin/ streptomycin). Fresh differentiation media were changed every 24 h until the end of the assay.

2.2. siRNA targeting *Ifitm1–3*

Small-interfering RNA directed against the mice *Ifitm1–3* was designed by siDirect (*http://sidirect2.rnai.jp/*) and was synthesized by GenePharma (Shanghai, China). ExFect transfection reagent (Vazyme, Nanjing, China), siRNAs, and negative controls (si-NC) were used to transfect C2C12 cells for 6 h. The cells were transfected using ExFect transfection reagent (Vazyme, Nanjing, China) following the manufacturer's instructions. Cells transfected with transfection reagent only were used as the mock control. Then, the supernatant was replaced by myogenic differentiation media as described above. The designed sense strand of siRNA was as follows: si1-*Ifitm1*: 5′-GCAGCAAGAGGUGGUUGUATT-3′; si2-*Ifitm1*: 5′-CAAGCUAUGAGACAAUCAATT-3′; si1-*Ifitm2*: 5′-GACAAUCAAAGAGGAGUATT-3′; si2-*Ifitm2*: 5′-GGGUCACCCCACAUCUCAATT-3′; si1-*Ifitm3*: 5′-CGAAAGAAUCAAGGAAGAATT-3′; si2-*Ifitm3*: GUUGUUAUCACCAUUGUUATT-3′.

2.3. RNA extraction and RT-qPCR

Total RNA from C2C12 cultured in differentiation and un-differentiation medium was isolated using FastGene RNA Basic Kit (Takara, Japan) in accordance with the manufacturer's instructions. RNA purity and integrity were evaluated using a NanoDrop-2000 spectrophotometer. After DNase I (Takara, Japan) digestion, total RNAs were reverse-transcribed to cDNA using ReverTra Ace qPCR RT Kit (Takara, Japan).

Table 1. Primer sequences for RT-qPCR

Primer	Primer sequence (5′-3′)
Mus-Ifitm1	F: GCTCCTCGACCACACCTCT
	R: TGGAGATCTCAGGCATGTTG
Mus-Ifitm2	F: TGGGCTTCGTTGCCTATGC
	R: AGAATGGGGTGTTCTTTGTGC
Mus-Ifitm3	F: CCCCCAAACTACGAAAGAATCA
	R: ACCATCTTCCGATCCCTAGAC
Mus-desmin	F: GTGAAGATGGCCTTGGATGT
	R: AAGGTCTGGATCGGAAGGTT
Mus-MyoD	F: AGCACTACAGTGGCGACTCA
	R: GGCCGCTGTAATCCATCAT
Mus-Myf5	F: CTGCTCTGAGCCCACCAG
	R: GACAGGGCTGTTACATTCAGG
Mus-myogenin	F: GAGACATCCCCCTATTTCTACCA
	R: GCTCAGTCCGCTCATAGCC
Mus-Gapdh	F: CATCCCAGAGCTGAACG
	R: CTGGTCCTCAGTGTAGCC

qPCR was performed using 2× SYBR Green qPCR Mix (SparkJade, Bio, China) with a Lightcycler 480. The PCR program was as follows: initial 5 min denaturation at 95°C, followed by 45 cycles of amplification at 95°C for 10 s, 60°C for 10 s, and 72°C for 15 s. To quantify the expression of each candidate gene, the mRNA expression levels were normalized to the level of glyceraldehyde 3-phosphate dehydrogenase (GAPDH) mRNA. Relative gene expression was calculated with the $2^{-\Delta\Delta Ct}$ method. Each sample was performed in triplicate. Sequences of the forward and reverse primers for RT-qPCR are shown in Table 1.

2.4. Western blotting

C2C12 cells in the six-well plate were washed with precooled phosphate buffer solution (PBS) and lysed with 200 μL of protein RIPA lysis buffer supplemented with 1% PMSF (CWBIO, China) per well for 1 h on ice. Then, the extracted precipitate was quantified using the BCA protein concentration assay kit (Biosharp, China). The processed protein samples (20 μg/line) were resolved using 12% SDS-PAGE at 60 V in the stacking gel and at 120 V in the separating gel. Proteins in the gels were transferred to polyvinylidene fluoride membranes (0.45 μm, Biosharp, China). The membranes were blocked with 5% skim milk in Tris-buffered saline containing 0.1% Tween 20 (TBST) for 2 h at room temperature, and then the membranes were incubated with primary antibodies, namely, rabbit anti-desmin (ab32362, Abcam, USA), rabbit anti-MyoD (ab203383, Abcam, USA), rabbit anti-MYF5 (ab125301, Abcam, USA), rabbit anti-IFITM1 (bs-1031R, Bioss, China), rabbit anti-IFITM2 (bs-15517R, Bioss, China), mouse anti-IFITM3 (bsm-51629M, Bioss, China), and rabbit anti-GAPDH (ab8245, Abcam, USA), at 4°C overnight. Then, the membranes were incubated in PBS-Tween containing anti-rabbit-horseradish peroxidase–conjugated secondary antibodies (SA00001, Proteintech, USA) for

1 h at 37°C. The membranes were washed in PBST, and signals of the protein blots were acquired using an ECL Chemiluminescence Substrate Kit (Biosharp, China) and visualized by exposing the membranes in a Chemiluminescence Gel Imaging System (18200880, Alliance, UK). The level of expression of each protein was normalized to that of GAPDH. The results were quantified using ImageJ-win64 software (Rawak Software Inc., Stuttgart, Germany).

2.5. Giemsa staining

C2C12 cells were gently washed with PBS three times and fixed with anhydrous methanol for 15 min. The Giemsa staining solutions were diluted with PBS. C2C12 cells were then incubated with the diluted staining solution for 15 min at 37°C and washed with PBS twice. Morphological observation was conducted using an inverted microscope. Images were taken randomly of three different sections per dish. The number of nuclei in myotubes and the total number of nuclei in the cells were counted in each field. Fusion indexes were calculated by expressing the number of nuclei in the myotubes as percentages of the total number of nuclei.

2.6. Immunoprecipitation

Co-immunoprecipitation was performed using the Pierce™ Classic Magnetic IP/Complex Immunoprecipitation (Co-IP) Kit (88804, Thermo, USA) in accordance with the manufacturer's protocol. Briefly, C2C12 cells were lysed with RIPA lysis buffer supplemented with 1% PMSF as described above. Then, 200 μL of the cell lysate was incubated with a mixture of 20 μL of protein A/G beads and 5 μL of conjugated antibody to IFITM1 or IFITM3 overnight with rotation at 4°C. The beads were then washed with IP (Immunoprecipitation) lysis/wash buffer and PBS. An aliquot of 200 μL of elution buffer was added to the beads, which were incubated at room temperature and mixed for 5–10 min. The supernatant was transferred to a new tube. Finally, the samples were loaded onto SDS-PAGE gel for LC-MS/MS analysis or western blot analysis.

2.7. LC-MS/MS analysis

Proteins in gel pieces were destained in 50 mM NH_4HCO_3 in 50% acetonitrile (v/v) until clear. Gel pieces were dehydrated with 100 μL of 100% acetonitrile for 5 min; the liquid was removed; and the gel pieces were rehydrated in 10 mM dithiothreitol and incubated at 56°C for 60 min. The gel pieces were again dehydrated in 100% acetonitrile; the liquid was removed; and the gel pieces were rehydrated with 55 mM iodoacetamide. The samples were incubated at room temperature for 45 min in the dark. The gel pieces were washed with 50 mM NH_4HCO_3 and dehydrated with 100% acetonitrile. They were rehydrated with 10 ng/μL trypsin resuspended in 50 mM NH_4HCO_3 on ice for 1 h. Excess liquid was removed, and the gel pieces were digested with trypsin at 37°C overnight. Peptides were extracted with 50% acetonitrile/5% formic acid, followed by 100% acetonitrile. Peptides were dried to completion and resuspended in 2% acetonitrile/0.1% formic acid.

The tryptic peptides were dissolved in 0.1% formic acid (solvent A) and directly loaded onto a home-made reversed-phase analytical column (15-cm length, 75 μm i.d.). The gradient comprised an increase from 6% to 23% solvent B (0.1% formic acid in 98% acetonitrile) over 16 min, a rise from 23% to 35% in 8 min, and climbing to 80% in 3 min, followed by holding at 80% for the last 3 min, all at a constant flow rate of 400 nL/min on an EASY-nLC 1000 UPLC system.

The peptides were subjected to NSI source followed by tandem mass spectrometry (MS/MS) in Q ExactiveTM Plus (Thermo) coupled online to the UPLC. The electrospray voltage applied was 2.0 kV. The m/z scan range was 350 to 1,800 for full scan, and intact peptides were detected in the Orbitrap at a resolution of 70,000. Peptides were then selected for MS/MS using NCE setting as 28 and the fragments were detected in the Orbitrap at a resolution of 17,500. A data-dependent procedure alternated between one MS scan followed by 20 MS/MS scans with 15.0 s dynamic exclusion. Automatic gain control (AGC) was set at 5E4.

The peptides were detected, isolated, and fragmented to produce a tandem mass spectrum of specific fragment ions for each peptide. The resulting MS/MS data were processed using Proteome Discoverer 1.3 and Uniprot database (*https://www.uniprot.org*).

2.8. Protein–protein interaction, KEGG, and GO enrichment analysis

A Venn diagram was drawn (*http://bioinformatics.psb.ugent.be/webtools/Venn*) to conduct an intersection analysis to compare binding proteins of IFITM1 and IFTM3. Protein–protein interaction was conducted by online String analysis (*https://string-db.org/*). A high confidence of 0.700 was set as the required score, and stringency was set as high (1%). Protein–protein interaction was clustered by kmeans. In addition, we performed Gene Ontology (GO) analysis. First, the data of function annotation diagram were obtained using the DAVID website (*https://david.ncifcrf.gov*), and the data with $P < 0.05$ were selected; the enriched paths were displayed using "tidyr" and "ggplot2" R packages. R package "cluster profiler" was used for GO enrichment analysis. Using the cnetplot function (circular = F, color edge = T, node tag = T), the data of GO analysis can be visualized as cnetplot. Data processing and mapping were performed using R-project (v4.0.5) and Rstudio

software (v1.3.1093).

2.9. Statistical analysis

The results are presented as the mean ± standard error of the mean (SEM). Statistical comparisons were made based on one-way ANOVA and Tukey's multiple-comparison test using GraphPad Prism software, version 7.0 (GraphPad Software Inc., San Diego, CA, USA), to)identify significant differences. P values < 0.05 were considered statistically significant (* represents $P < 0.05$, ** represents $P < 0.01$, *** represents $P < 0.001$). All experiments were performed at least three times.

3. Results

3.1. The increased expression of IFITMs in myogenic differentiation of C2C12 cells

The essential step in myogenesis is cell fusion and the formation of myotubes, whereby mononuclear myocytes fuse to form multinucleated myotubes. As expected, the number of fusing myocytes and myotubes increased on the subsequent induction day (Figure 1A and 1B). Gene and protein expression levels of desmin, Myf5, myogein, and MyoD on days 3, 5, and 7 after myogenic differentiation induction were consistent and significantly increased (Figure 1C–E).

The results of RT-PCR analysis indicated that the expression levels of *Ifitm1–3* increased during the differentiation of C2C12 cells. The differentiation medium stimulated the expression of *Ifitm1–3*, with the higher levels observed on the third day and thereafter (Figure 2A). Overall trends showed an increase in the expression of IFITM1–3 proteins in the differentiation process of C2C12 cells, with the higher values on days 3 and 7 compared with that on day 0 before myogenic induction. For IFITM1, decreased expression was observed on day 5, compared with day 3, and then climbed to the highest value on day 7. Protein level of IFITM2 was higher on days 3, 5, and 7 than on day 0 in the process of myogenic differentiation. IFITM3 expression was not significantly increased on day 5 compared with day 3, but there was an obvious increasing trend on day 7 (Figure 2B–C).

3.2. si-RNA knocks down the expression of *Ifitm1–3* in myogenic differentiation of C2C12 cells

Theoretically, the upregulated *Ifitm1–3* during the process of myogenic induction could be blocked by targeting *Ifitms* with small-interfering RNA (siRNA). Hence, we initially screened the siRNAs with high inhibition efficiency for targeting *Ifitm1–3*. The interference efficiency of siRNAs was determined to be over 70% as identified by RT-qPCR (Supplementary Figure S1, *http://www.irdrjournal.com/action/getSupplementalData.php?ID=152). Myotube formation was also evaluated*

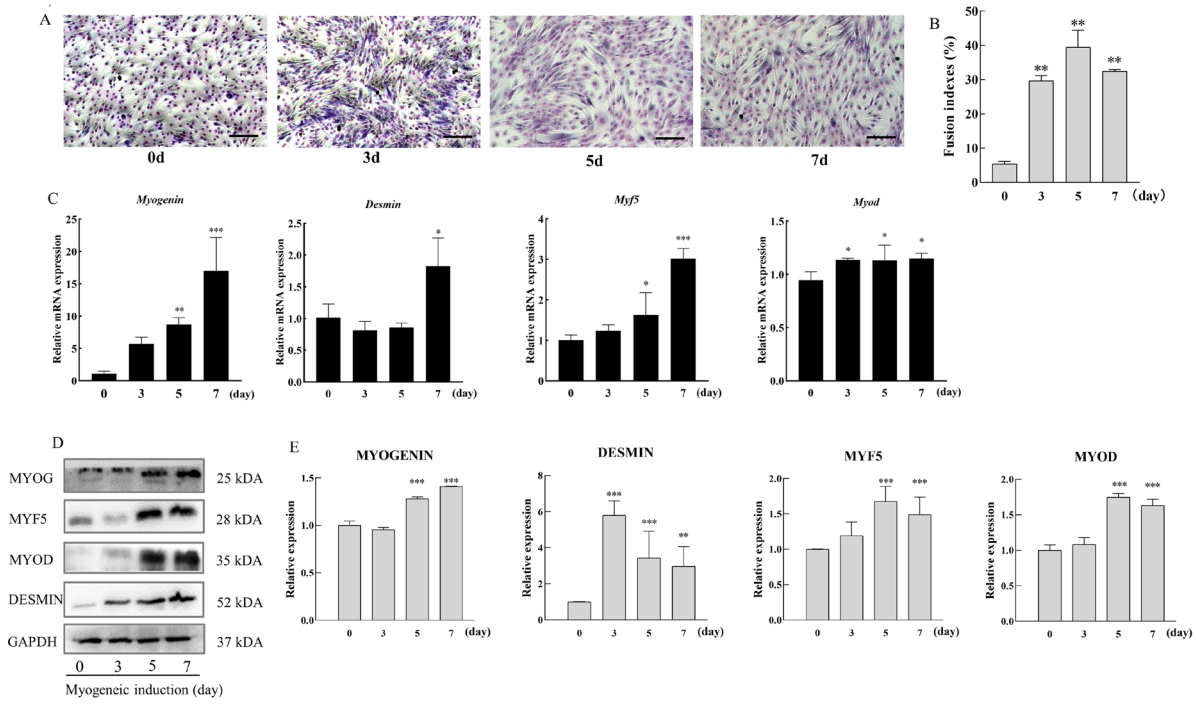

Figure 1. Myogenic differentiation of C2C12 myoblasts on days 0, 3, 5, and 7. (A) Microscopic images of C2C12 cells (stained by Giemsa staining prior to induction) and myoblasts. Magnification: 100×. **(B)** Relative expression of myogenin, myogenic differentiation factor D (MyoD), Myf5, and desmin mRNA as measured by qRT-PCR. **(C)** Representative bands for myogenin, MyoD, Myf5, desmin, and GAPDH are shown. **(D)** Quantification of band intensity as described above is shown. The level of proteins was normalized to that of GAPDH. Statistical significance: *P <0.05; **P <0.01; ***P <0.001; NS, not significant.

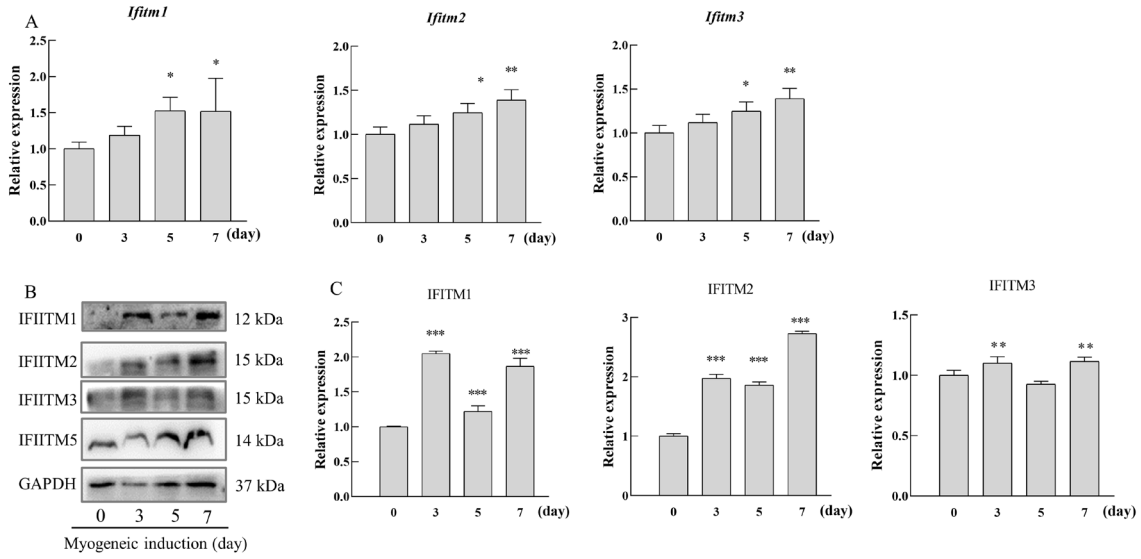

Figure 2. Increased expression of IFITM1–3 during myogenic differentiation of C2C12 myoblasts. (A) Relative expression of *Ifitm1–3* during the myogenic differentiation process. (B) Western blot evaluating the protein levels of IFITM1–3. (C) Quantification of band intensity as described above is shown. The level of proteins was normalized to that of GAPDH. Statistical significance: **P* < 0.05; ***P* < 0.01; ****P* < 0.001; NS, not significant.

*as the f*usion index. By the transfection of specific siRNA1 and siRNA2 targeting *Ifitm1–3* respectively, the percentage of fusion index decreased significantly in the interference groups of *Ifitm1–3*, compared with Mock group (Figure 3A–B). Especially in the *si2-Ifitm1* group, the percentage of fusion index decreased to 14.82% (*P* < 0.01%) (Figure 3B). Consistent with that, the expression of MyoD, myogenin, MYF5, and desmin was significantly repressed with differentiation in the *Ifitm1–3* knockdown groups as shown by western blot (Figure 3C–D).

3.3. Interacting proteins of IFITMs and GO enrichment analysis

In order to determine the interaction proteins of IFITM1–3, we performed immunoprecipitation–mass spectrometry (IP-MS) assays using IFITM1 and IFITM3 antibodies. Specific bands identified exclusively in the pull-down products of antibodies were excised for protein identification using MS (Figure 4A). A total of 84 proteins, including myosin, actin, vimentin, desmin, myosin regulatory light chain 12B, tropomyosin, and nucleolin (Table 2), were repeatedly identified in all three biological replicates. String analysis revealed 82 nodes, with an average node degree of 13.1. Clustering analysis identified three distinctive groups as follows: the cluster with green color included proteins involved in the process of muscle filament sliding and constituent proteins of sarcomere; the cluster with red color included ribosomal proteins; and the cluster in blue color included the heterogeneous nuclear ribonucleoprotein, histones, and proteins that regulate mRNA metabolic process (Figure 4B). We further validated and confirmed that desmin identified through IP-MS was indeed a bona fide interacting partner of IFITM1 and IFITM3 (Figure 4C).

The KEGG pathway analysis showed that the genes were mainly enriched in hypertrophic cardiomyopathy, dilated cardiomyopathy, cardiac muscle contraction, adrenergic signaling in cardiomyocytes, mRNA surveillance pathway, and RNA transport pathways (Figure 5A). The GO enrichment analyses revealed 329 biological process (BP) entries, involving ribonucleoprotein complex biogenesis, non-membrane-bounded organelle assembly, ribosome biogenesis, actin filament organization, muscle contraction, ncRNA processing, RNA splicing, and muscle system process (Figure 5B); 124 cell component (CC) entries, involving ribosomal subunit, ribosome, cell leading edge, large and small ribosomal subunit, postsynaptic density, asymmetric synapse, postsynaptic specialization, neuron to neuron synapse, contractile fiber, myofibril, myosin complex, stress fiber, contractile actin filament bundle, actin filament bundle actomyosin, and myosin II complex (Figure 5C); and 71 molecular function (MF) entries, involving structural constituent of ribosome, actin binding, actin filament binding, mRNA binding, rRNA binding, structural constituent of cytoskeleton, and cytoskeletal motor activity (Figure 5D).

4. Discussion

The functions of IFITMs are not sufficiently understood. IFITM1–3 inhibit viral fusion and cell entry with a broad virus spectrum. Our study identified that IFITM1–3 were involved in myogenesis and that they were upregulated in this process. The high expression of *Ifitm1–3* has also been reported in the differentiation of H92C cells, a rat

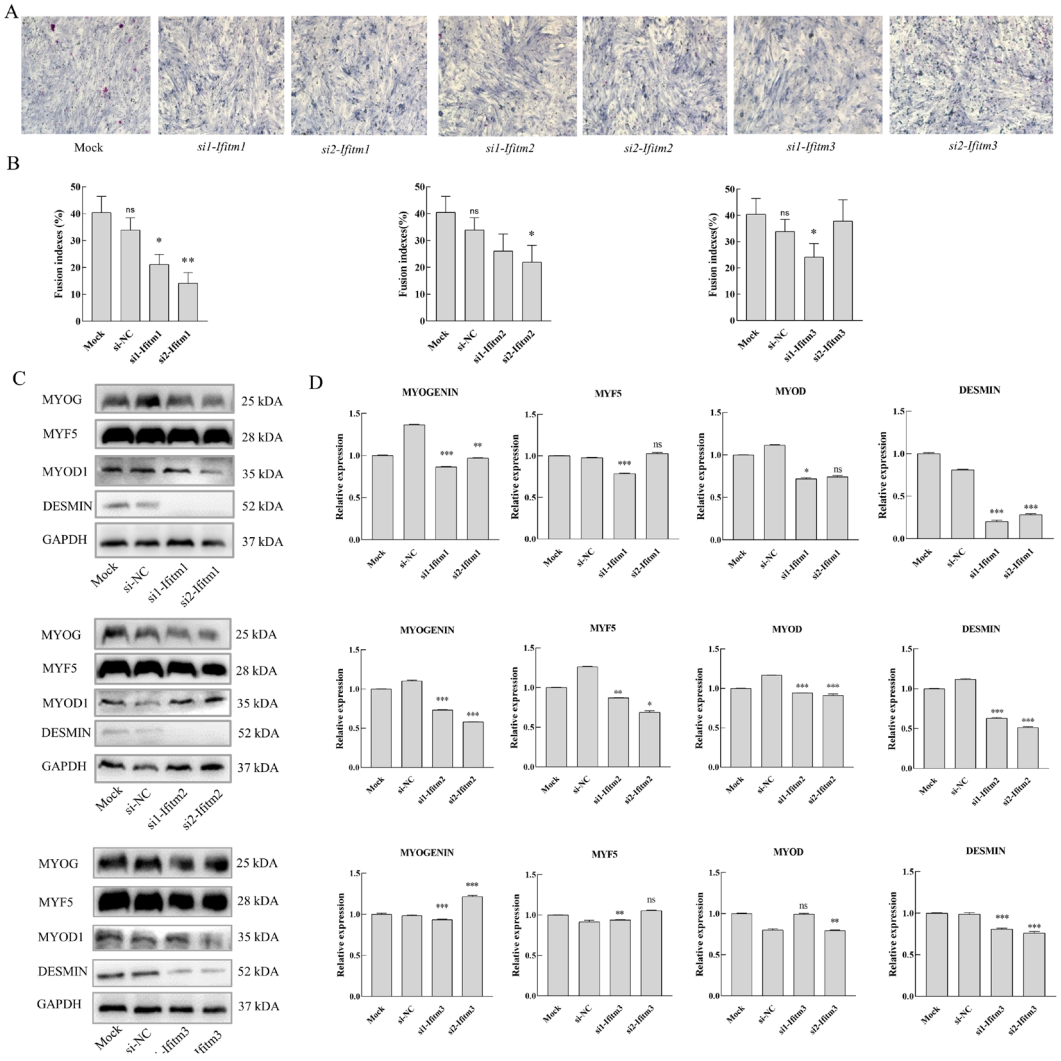

Figure 3. Knockdown of Ifitm1, 2, and 3 by siRNAs blocks myogenic differentiation in C2C12 cells. (A) Microscopic images of Giemsa staining for C2C12 myoblasts on day 3 of myogenic differentiation after transfection with siRNAs targeting *Ifitm1–3*. Two different siRNAs were used for each targeting gene. Transfection without siRNAs, but with transfection reagent was set as mock. Magnification: 100×. (B) Percentage fusion on day 3 of myogenic induction and transfection with siRNAs as described above, calculated by dividing the number of nuclei within multinucleated myofibers by the total number of nuclei. NC represents the group without siRNAs and transfection reagents. (C) Downregulated protein expression of myogenin, MyoD, Myf5, and desmin after interference by siRNAs targeting *Ifitm1–3.* (D) Quantification of band intensity as described above is shown. The level of proteins was normalized to that of GAPDH. Statistical significance: **P*<0.05; ***P* <0.01; ****P* <0.001; NS, not significant.

myoblast cell line (*37*).

IFITMs belong to the CD225 family of proteins. They consist of a conserved intracellular loop between the intramembrane domain and the transmembrane helix (*38,39*). Interaction proteins of IFITMs in different cell lines have been reported, including BRI3, SERINC5, and CAV-1 (*40-42*). All these molecules are related to antiviral effects. In this study, we uncovered that the interacting proteins of IFITM1 and IFITM3 clustered into cytoskeleton proteins ankycorbin, nestin, vimentin, actin, myosin, and desmin.

The sarcomere is the smallest functional unit of muscle fibers in the skeletal muscle, which is arranged between two Z-lines. The constituent proteins of the sarcomere include contractile proteins actin and myosin, structural proteins titin and nebulin, and intermediate filaments (*43*). Notably, we found that IFITM1 and IFITM3 interact with all these cytoskeleton proteins. Desmin encodes a muscle-specific class III intermediate filament and plays an essential role in muscular structure and function. Homopolymers of the protein form a stable intracytoplasmic filamentous network that connects myofibrils to each other and to the plasma membrane (*44*). As one of the earliest markers of an initial step in myogenic differentiation, the expression of desmin precedes the expression of all other muscle-specific structural genes and myogenic helix-loop-helix transcription factors MyoD, myogenin, and Mrf4 (*45*). In desmin-null mutant embryonic stem cell–derived embryoid bodies, skeletal and smooth muscle myogenesis were completely inhibited, displaying the absence of myotube formation, contractility, and expression of MyoD, myogenin, Myf5, and myosin heavy chain (*46*). In desmin-knockout mice, the loss of sarcomere integrity

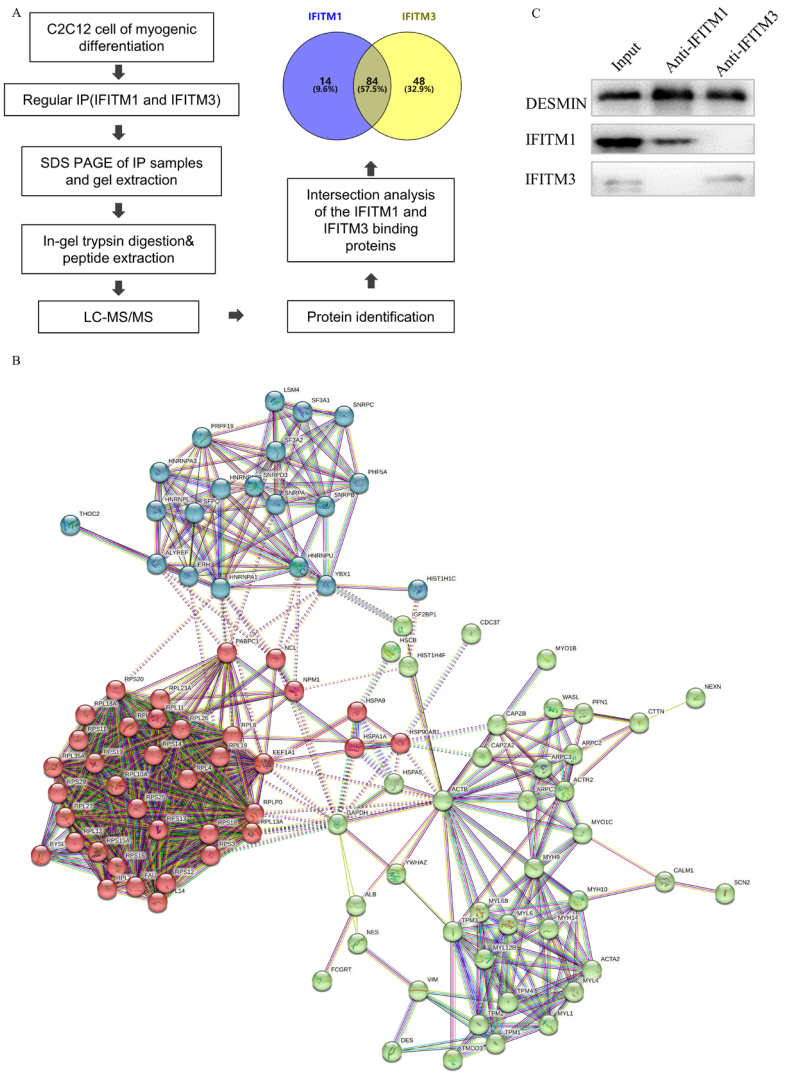

Figure 4. Identification and validation of IFITM1,3-interacting proteins. (A) Principle of co-immunoprecipitation and liquid chromatography combined with tandem mass spectrometry (LC–MS/MS). (B) The protein–protein interaction network if IFITM1,3 (overlapped) revealed by STRING analysis. A total of 84 unique homologous proteins are shown in the network. Three clusters are indicated in different colors. Cluster 1: muscle filament sliding (green color); Cluster 2: ribosome series proteins (red color); Cluster 3: regulation of mRNA metabolic process (blue color). Associations are represented by the lines. Thicker lines represent stronger associations. (C) Co-IP assays show the interaction between desmin and IFITM1, 3.

and the increased number of mitochondria in myofibers were obvious. A reduced gain of muscle performance was observed in mechanical-overload mice that lacked desmin (*47*). Desmin is the pathogenic gene for dilated cardiomyopathy-1I, myofibrillar myopathy-1, and neurogenic scapuloperoneal syndrome (*48-50*). Desmin-null mice demonstrate a multisystem disorder that involves cardiac, skeletal, and smooth muscles at the early stage of their postnatal life (*51*). During murine feto-embryonic development, there is coexpression of desmin and α-actin in skeletal muscle cells, while the expression of desmin precedes that of α-actin in myoblasts of somites (*52*).

Vimentin and nestin also belong to intermediate filaments that participate in the formation of cytoskeleton and maintenance of cell morphology. Vimentin is poorly expressed during myogenic differentiation as it is replaced by the tissue-specific intermediate filament protein, desmin (*53*). Nestin regulates the differentiation of myogenic precursor cells by Cdk5 and it is downregulated in myoblasts (*54,55*). Nestin-knockout mice have a spontaneous regenerative phenotype in skeletal muscle, which is related to a disturbed proliferation cycle under the uncontrolled Cdk5 kinase activity (*54*). Sliding movement between myosin and actin is the molecular basis of muscle contraction. These two proteins are also involved in cytokinesis, locomotion, cell motility, and maintenance of cell shape (*56,57*).

The functions of IFITMs in oncogenesis have been explored in recent years. IFITM3 binds to PIP3 to amplify PIP3 signaling and Src-kinase signaling in B cells by interacting with activated B-cell receptor (BCR) complex. Phosphorylation of Ifitm3-Y20 transfers the location of endosome to the cell surface, thereby initiating the amplification loop of oncogenic signaling (*58*). IFITM3 is involved in gastric cancer, hepatocellular carcinoma, and prostate cancer through the MET/AKT/FOXO3/c-MYC axis, p38/MAPK signaling, and TGF-β signaling pathway, respectively (*30,59,60*).

Our study showed the interaction proteins of IFITMs and their involvement in the myogenic differentiation. Although further studies need to explore the molecular

Table 2. Overlapped interacted proteins for IFITM1 and IFITM3

	Accession	Protein names	Gene names	MW [kDa]
1	Q8VDD5	Myosin-9	*Myh9*	226.23
2	Q61879	Myosin-10	*Myh10*	228.85
3	P60710	Actin, cytoplasmic 1	*Actb*	41.71
4	P62737	Actin, aortic smooth muscle	*Acta2*	41.98
5	P20152	Vimentin	*Vim*	53.66
6	P31001	Desmin	*Des*	53.47
7	Q3THE2	Myosin regulatory light chain 12B	*Myl12b*	19.77
8	Q60605	Myosin light polypeptide 6	*Myl6*	16.92
9	P58774	Tropomyosin beta chain	*Tpm2*	32.82
10	Q6URW6	Myosin-14	*Myh14*	228.45
11	P58771	Tropomyosin alpha-1 chain	*Tpm1*	32.66
12	P09405	Nucleolin	*Ncl*	76.68
13	P21107	Tropomyosin alpha-3 chain	*Tpm3*	32.97
14	Q61937	Nucleophosmin	*Npm1*	32.54
15	P05977	Myosin light chain 1/3, skeletal muscle isoform	*Myl1*	20.58
16	P0DP26	Calmodulin-1	*Calm1*	16.83
17	Q9ERG0	LIM domain and actin-binding protein 1	*Lima1*	84.01
18	Q6IRU2	Tropomyosin alpha-4 chain	*Tpm4*	28.45
19	Q9WTI7	Unconventional myosin-Ic	*Myo1c*	121.87
20	P47757	F-actin-capping protein subunit beta	*Capzb*	31.33
21	P07724	Albumin	*Alb*	68.65
22	Q9EP71	Ankycorbin	*Rai14*	108.79
23	P49312	Heterogeneous nuclear ribonucleoprotein A1	*Hnrnpa1*	34.18
24	Q6P5H2	Nestin	*Nes*	207.00
25	P10126	Elongation factor 1-alpha 1	*Eef1a1*	50.08
26	Q61696	Heat shock 70 kDa protein 1A	*Hspa1a*	70.04
27	Q9CZX8	40S ribosomal protein S19	*Rps19*	16.08
28	P67984	60S ribosomal protein L22	*Rpl22*	14.75
29	P01942	Hemoglobin subunit alpha	*Hba*	15.08
30	P62908	40S ribosomal protein S3	*Rps3*	26.66
31	P62852	40S ribosomal protein S25	*Rps25*	13.73
32	Q60598	Src substrate cortactin	*Cttn*	61.21
33	P62960	Y-box-binding protein 1	*Ybx1*	35.71
34	Q9JHJ0	Tropomodulin-3	*Tmod3*	39.48
35	P35979	60S ribosomal protein L12	*Rpl12*	17.79
36	Q91WK0	Leucine-rich repeat flightless-interacting protein 2	*Lrrfip2*	47.12
37	P20029	Endoplasmic reticulum chaperone BiP	*Hspa5*	72.38
38	P15864	Histone H1.2	*H1-2*	21.25
39	P62862	40S ribosomal protein S30	*Fau*	6.64
40	Q9CR57	60S ribosomal protein L14	*Rpl14*	23.55
41	P29341	Polyadenylate-binding protein 1	*Pabpc1*	70.63
42	P62270	40S ribosomal protein S18	*Rps18*	17.71
43	Q8CI43	Myosin light chain 6B	*Myl6b*	22.73
44	Q8VIJ6	Splicing factor, proline- and glutamine-rich	*Sfpq*	75.39
45	P62264	40S ribosomal protein S14	*Rps14*	16.26
46	P62301	40S ribosomal protein S13	*Rps13*	17.21
47	O88569	Heterogeneous nuclear ribonucleoproteins A2/B1	*Hnrnpa2b1*	37.38
48	P63101	14-3-3 protein zeta/delta	*Ywhaz*	27.75
49	P62806	Histone H4	*H4c1*	11.36
50	Q9D8E6	60S ribosomal protein L4	*Rpl4*	47.12
51	P11499	Heat shock protein HSP 90-beta	*Hsp90ab1*	83.23
52	P61161	Actin-related protein 2	*Actr2*	44.73
53	P09541	Myosin light chain 4	*Myl4*	21.15
54	P84089	Enhancer of rudimentary homolog	*Erh*	12.25
55	P47754	F-actin-capping protein subunit alpha-2	*Capza2*	32.95
56	P61358	60S ribosomal protein L27	*Rpl27*	15.79
57	P62751	60S ribosomal protein L23a	*Rpl23a*	17.68
58	P19253	60S ribosomal protein L13a	*Rpl13a*	23.45
59	O08583	THO complex subunit 4	*Alyref*	26.92
60	P60867	40S ribosomal protein S20	*Rps20*	13.36
61	P53026	60S ribosomal protein L10a	*Rpl10a*	24.90
62	P62274	40S ribosomal protein S29	*Rps29*	6.67
63	P62245	40S ribosomal protein S15a	*Rps15a*	14.83
64	P02088	Hemoglobin subunit beta-1	*Hbb-b1*	15.83
65	Q9CXW4	60S ribosomal protein L11	*Rpl11*	20.24
66	P46735	Unconventional myosin-Ib	*Myo1b*	128.48
67	Q8BG05	Heterogeneous nuclear ribonucleoprotein A3	*Hnrnpa3*	39.63

Table 2. Overlapped interacted proteins for IFITM1 and IFITM3 (continued)

	Accession	Protein names	Gene names	MW [kDa]
68	Q7TPW1	Nexilin	*Nexn*	72.06
69	O55142	60S ribosomal protein L35a	*Rpl35a*	12.55
70	P14131	40S ribosomal protein S16	*Rps16*	16.44
71	P14869	60S acidic ribosomal protein P0	*Rplp0*	34.19
72	P61514	60S ribosomal protein L37a	*Rpl37a*	10.27
73	Q61495	Desmoglein-1-alpha	*Dsg1a*	114.52
74	Q9WV32	Actin-related protein 2/3 complex subunit 1B	*Arpc1b*	41.04
75	Q9CVB6	Actin-related protein 2/3 complex subunit 2	*Arpc2*	34.34
76	Q8VEK3	Heterogeneous nuclear ribonucleoprotein U	*Hnrnpu*	87.86
77	Q9QXA5	U6 snRNA-associated Sm-like protein LSm4	*Lsm4*	15.07
78	P27048	Small nuclear ribonucleoprotein-associated protein B	*Snrpb*	23.64
79	P61255	60S ribosomal protein L26	*Rpl26*	17.25
80	P47911	60S ribosomal protein L6	*Rpl6*	33.49
81	P38647	Stress-70 protein, mitochondrial	*Hspa9*	73.42
82	E9Q3S4	Mitogen-activated protein kinase kinase kinase 19	*Map3k19*	146.32
83	P62281	40S ribosomal protein S11	*Rps11*	18.42
84	O88477	Insulin-like growth factor 2 mRNA-binding protein 1	*Igf2bp1*	63.41

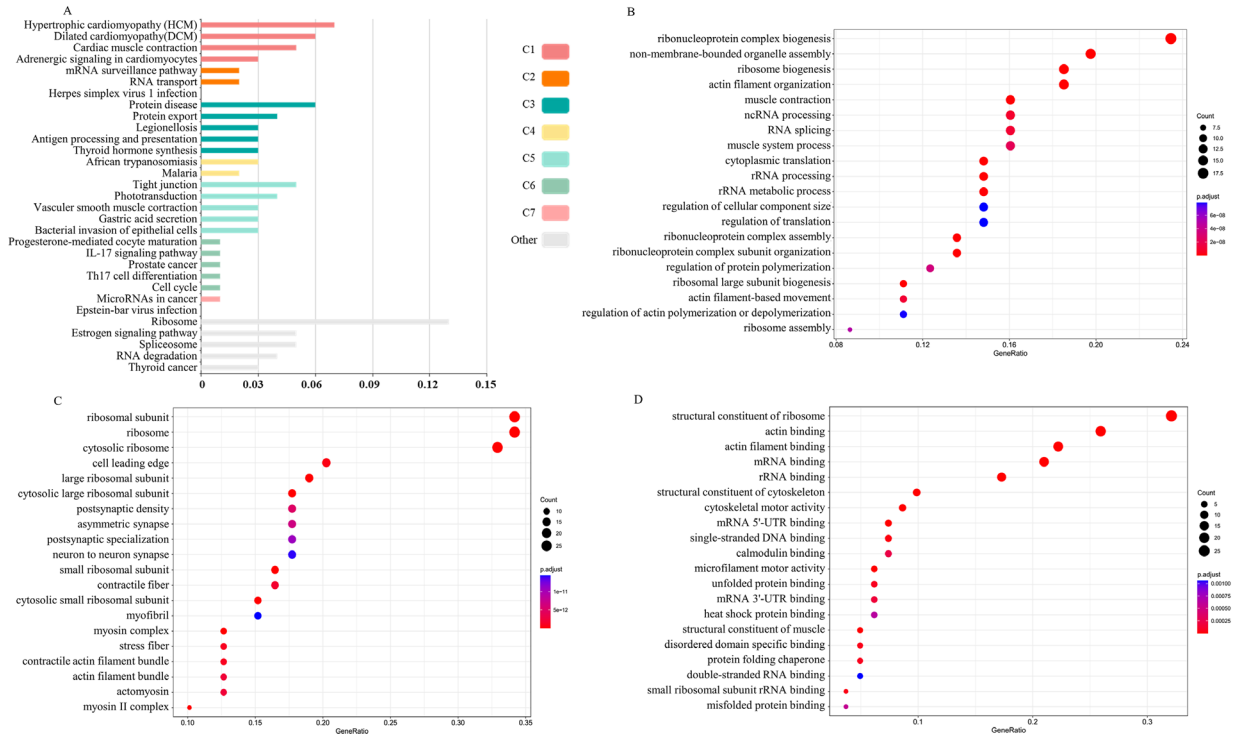

Figure 5. GO and KEGG pathway enrichment analysis of 84 proteins that interact with IFITM1, 3 (overlapped). (A) KEGG classification map of differentially expressed genes. The y-axis shows the metabolic pathway. (B) Biological process (BP). (C) Cellular component (CC). (D) Molecular function (MF). The x-axis represents gene ratio = count/set size. Dot size represents the number of genes, and the color bar represents the P_{adj}-value.

mechanisms of IFITMs, we hypothesize that cytoskeletal proteins desmin, actin, myosin, vimentin, and nestin may function as scaffolds to enroll IFITMs, thereby interacting with IFITM1 and IFITM3. Desmin regulates myoblast differentiation through its downstream myogenic determination factors MyoD, Mrf4, and myogenin, which serve as differentiation factors. Our results provide insight into the molecular mechanisms of Ifitm-mediated myogenic differentiation and may facilitate the development of future treatments for myotrophic diseases.

Funding: This work was supported by a grant from Academic Promotion Program of Shandong First Medical University (LJ001).

Conflict of Interest: The authors have no conflicts of interest to disclose.

References

1. Zhao X, Li J, Winkler CA, An P, Guo JT. IFITM Genes, Variants, and Their Roles in the Control and Pathogenesis

of Viral Infections. Front Microbiol. 2018; 9:3228.
2. Liao Y, Goraya MU, Yuan X, Zhang B, Chiu SH, Chen JL. Functional Involvement of Interferon-Inducible Transmembrane Proteins in Antiviral Immunity. Front Microbiol. 2019; 10:1097.
3. Lewin AR, Reid LE, McMahon M, Stark GR, Kerr IM. Molecular analysis of a human interferon-inducible gene family. Eur J Biochem. 1991; 199:417-423.
4. Bedford JG, O'Keeffe M, Reading PC, Wakim LM. Rapid interferon independent expression of IFITM3 following T cell activation protects cells from influenza virus infection. PLoS One. 2019; 14:e0210132.
5. Wakim LM, Gupta N, Mintern JD, Villadangos JA. Enhanced survival of lung tissue-resident memory $CD8^+$ T cells during infection with influenza virus due to selective expression of IFITM3. Nat Immunol. 2013; 14:238-245.
6. Amet T, Son YM, Jiang L, Cheon IS, Huang S, Gupta SK, Dent AL, Montaner LJ, Yu Q, Sun J. BCL6 represses antiviral resistance in follicular T helper cells. Journal of leukocyte biology. 2017; 102:527-536.
7. Yánez DC, Sahni H, Ross S, *et al*. IFITM proteins drive type 2 T helper cell differentiation and exacerbate allergic airway inflammation. European journal of immunology. 2019; 49:66-78.
8. Kim YC, Won SY, Jeong BH. The first association study of single-nucleotide polymorphisms (SNPs) of the IFITM1 gene with influenza H1N1 2009 pandemic virus infection. Molecular & cellular toxicology. 2021; 17:179-186.
9. Prelli Bozzo C, Nchioua R, Volcic M, *et al*. IFITM proteins promote SARS-CoV-2 infection and are targets for virus inhibition *in vitro*. Nature communications. 2021; 12:4584.
10. Reid LE, Brasnett AH, Gilbert CS, Porter AC, Gewert DR, Stark GR, Kerr IM. A single DNA response element can confer inducibility by both alpha- and gamma-interferons. Proceedings of the National Academy of Sciences of the United States of America. 1989; 86:840-844.
11. Lu J, Pan Q, Rong L, He W, Liu SL, Liang C. The IFITM proteins inhibit HIV-1 infection. J Virol. 2011; 85:2126-2137.
12. Savidis G, Perreira JM, Portmann JM, Meraner P, Guo Z, Green S, Brass AL. The IFITMs Inhibit Zika Virus Replication. Cell Rep. 2016; 15:2323-2330.
13. Raychoudhuri A, Shrivastava S, Steele R, Kim H, Ray R, Ray RB. ISG56 and IFITM1 proteins inhibit hepatitis C virus replication. J Virol. 2011; 85:12881-12889.
14. Tanaka SS, Matsui Y. Developmentally regulated expression of mil-1 and mil-2, mouse interferon-induced transmembrane protein like genes, during formation and differentiation of primordial germ cells. Gene Expr Patterns. 2002; 2:297-303.
15. Lange UC, Saitou M, Western PS, Barton SC, Surani MA. The fragilis interferon-inducible gene family of transmembrane proteins is associated with germ cell specification in mice. BMC Dev Biol. 2003; 3:1.
16. Buchrieser J, Degrelle SA, Couderc T, *et al*. IFITM proteins inhibit placental syncytiotrophoblast formation and promote fetal demise Interferon-induced transmembrane proteins inhibit cell fusion mediated by trophoblast syncytins. Science. 2019; 365:176-180.
17. Zani A, Zhang L, McMichael TM, Kenney AD, Chemudupati M, Kwiek JJ, Liu SL, Yount JS. Interferon-induced transmembrane proteins inhibit cell fusion mediated by trophoblast syncytins. J Biol Chem. 2019; 294:19844-19851.
18. Lange UC, Adams DJ, Lee C, Barton S, Schneider R, Bradley A, Surani MA. Normal germ line establishment in mice carrying a deletion of the Ifitm/Fragilis gene family cluster. Molecular and cellular biology. 2008; 28:4688-4696.
19. Hanagata N. IFITM5 mutations and osteogenesis imperfecta. Journal of bone and mineral metabolism. 2016; 34:123-131.
20. Hedjazi G, Guterman-Ram G, Blouin S, Schemenz V, Wagermaier W, Fratzl P, Hartmann MA, Zwerina J, Fratzl-Zelman N, Marini JC. Alterations of bone material properties in growing Ifitm5/BRIL p.S42 knock-in mice, a new model for atypical type VI osteogenesis imperfecta. Bone. 2022; 162:116451.
21. Tyurin A, Merkuryeva E, Zaripova A, Markova T, Nagornova T, Dantsev I, Nadyrshina D, Zakharova E, Khusainova R. Does the c.-14C>T Mutation in the IFITM5 Gene Provide Identical Phenotypes for Osteogenesis Imperfecta Type V? Data from Russia and a Literature Review. Biomedicines. 2022; 10.
22. Shapiro JR, Lietman C, Grover M, *et al*. Phenotypic variability of osteogenesis imperfecta type V caused by an IFITM5 mutation. Journal of bone and mineral research : the official journal of the American Society for Bone and Mineral Research. 2013; 28:1523-1530.
23. Wang D, Wang D, Huang M, *et al*. Transcriptomic characteristics and impaired immune function of patients who retest positive for SARS-CoV-2 RNA. J Mol Cell Biol. 2021; 13:748-759.
24. Kelemen A, Carmi I, Oszvald Á, Lőrincz P, Petővári G, Tölgyes T, Dede K, Bursics A, Buzás EI, Wiener Z. IFITM1 expression determines extracellular vesicle uptake in colorectal cancer. Cell Mol Life Sci. 2021; 78:7009-7024.
25. Gómez-Herranz M, Faktor J, Yébenes Mayordomo M, Pilch M, Nekulova M, Hernychova L, Ball KL, Vojtesek B, Hupp TR, Kote S. Emergent Role of IFITM1/3 towards Splicing Factor (SRSF1) and Antigen-Presenting Molecule (HLA-B) in Cervical Cancer. Biomolecules. 2022; 12.
26. Yu F, Xie D, Ng SS, Lum CT, Cai MY, Cheung WK, Kung HF, Lin G, Wang X, Lin MC. IFITM1 promotes the metastasis of human colorectal cancer *via* CAV-1. Cancer Lett. 2015; 368:135-143.
27. Yan J, Jiang Y, Lu J, Wu J, Zhang M. Inhibiting of Proliferation, Migration, and Invasion in Lung Cancer Induced by Silencing Interferon-Induced Transmembrane Protein 1 (IFITM1). Biomed Res Int. 2019; 2019:9085435.
28. Xu L, Zhou R, Yuan L, Wang S, Li X, Ma H, Zhou M, Pan C, Zhang J, Huang N, Shi M, Bin J, Liao Y, Liao W. IGF1/IGF1R/STAT3 signaling-inducible IFITM2 promotes gastric cancer growth and metastasis. Cancer Lett. 2017; 393:76-85.
29. De Marco M, Basile A, Iorio V, *et al*. Role of BAG3 in cancer progression: A therapeutic opportunity. Semin Cell Dev Biol. 2018; 78:85-92.
30. Liu X, Chen L, Fan Y, Hong Y, Yang X, Li Y, Lu J, Lv J, Pan X, Qu F, Cui X, Gao Y, Xu D. IFITM3 promotes bone metastasis of prostate cancer cells by mediating activation of the TGF-β signaling pathway. Cell Death Dis. 2019; 10:517.
31. Liu Y, Lu R, Cui W, *et al*. High IFITM3 expression predicts adverse prognosis in acute myeloid leukemia. Cancer Gene Ther. 2020; 27:38-44.
32. Liu Y, Liu J, Tian Z, Zhang Z, Liu T, Chen C, Tang X, Zhu J. Highly expressed IFITM10 is associated with early

diagnosis and T stage of gastric cancer. Transl Cancer Res. 2021; 10:382-392.
33. Agarwal M, Sharma A, Kumar P, Kumar A, Bharadwaj A, Saini M, Kardon G, Mathew SA-O. Myosin heavy chain-embryonic regulates skeletal muscle differentiation during mammalian development. LID - 10.1242/dev.184507 [doi] LID - dev184507.
34. Costa ML, Escaleira R, Cataldo A, Oliveira F, Mermelstein CS. Desmin: molecular interactions and putative functions of the muscle intermediate filament protein. Brazilian journal of medical and biological research = Revista brasileira de pesquisas medicas e biologicas. 2004; 37:1819-1830.
35. Costa ML, Escaleira R, Manasfi M, de Souza LF, Mermelstein CS. Cytoskeletal and cellular adhesion proteins in zebrafish (Danio rerio) myogenesis. Brazilian journal of medical and biological research = Revista brasileira de pesquisas medicas e biologicas. 2003; 36:1117-1120.
36. Zammit PS. Function of the myogenic regulatory factors Myf5, MyoD, Myogenin and MRF4 in skeletal muscle, satellite cells and regenerative myogenesis.
37. Lau SL, Yuen ML, Kou CY, Au KW, Zhou J, Tsui SK. Interferons induce the expression of IFITM1 and IFITM3 and suppress the proliferation of rat neonatal cardiomyocytes. J Cell Biochem. 2012; 113:841-847.
38. Ling SL, Zhang CW, Wang W, Cai XY, Yu L, Wu FM, Zhang LH, Tian CL. Combined approaches of EPR and NMR illustrate only one transmembrane helix in the human IFITM3. Scientific Reports. 2016; 6.
39. Zhao XS, Li JR, Winkler CA, An P, Guo JT. IFITM Genes, Variants, and Their Roles in the Control and Pathogenesis of Viral Infections. Frontiers in Microbiology. 2019; 9.
40. Akiva İ, Birgül Iyison N. Identification of IFITM3 and MGAT1 as novel interaction partners of BRI3 by yeast two-hybrid screening. Turkish journal of biology = Turk biyoloji dergisi. 2018; 42:463-470.
41. Li W, Zhang Z, Zhang L, Zhou Q, Li Y, Yi L, Ding H, Zhao M, Chen J, Fan S. Interaction of SERINC5 and IFITM1/2/3 regulates the autophagy-apoptosis-immune network under CSFV infection. Virulence. 2022; 13:1720-1740.
42. Xu Y, Yang G, Hu G. Binding of IFITM1 enhances the inhibiting effect of caveolin-1 on ERK activation. Acta Biochim Biophys Sin (Shanghai). 2009; 41:488-494.
43. Marzuca-Nassr G, Vitzel K, Mancilla-Solorza E, Márquez J. Sarcomere Structure: The Importance of Desmin Protein in Muscle Atrophy. International Journal of Morphology. 2018; 36:576-583.
44. Hnia K, Ramspacher C, Vermot J, Laporte J. Desmin in muscle and associated diseases: beyond the structural function. Cell Tissue Res. 2015; 360:591-608.
45. Sassoon DA. Myogenic regulatory factors: dissecting their role and regulation during vertebrate embryogenesis. Dev Biol. 1993; 156:11-23.
46. Weitzer G, Milner DJ, Kim JU, Bradley A, Capetanaki Y. Cytoskeletal control of myogenesis: a desmin null mutation blocks the myogenic pathway during embryonic stem cell differentiation. Dev Biol. 1995; 172:422-439.
47. Joanne P, Hovhannisyan Y, Bencze M, Daher MT, Parlakian A, Toutirais G, Gao-Li J, Lilienbaum A, Li Z, Kordeli E, Ferry A, Agbulut O. Absence of Desmin Results in Impaired Adaptive Response to Mechanical Overloading of Skeletal Muscle. Front Cell Dev Biol. 2021; 9:662133.
48. Taylor MR, Slavov D, Ku L, *et al*. Prevalence of desmin mutations in dilated cardiomyopathy. Circulation. 2007; 115:1244-1251.
49. Ojrzyńska N, Bilińska ZT, Franaszczyk M, Płoski R, Grzybowski J. Restrictive cardiomyopathy due to novel desmin gene mutation. Kardiologia polska. 2017; 75:723.
50. Walter MC, Reilich P, Huebner A, Fischer D, Schroder R, Vorgerd M, Kress W, Born C, Schoser BG, Krause KH, Klutzny U, Bulst S, Frey JR, Lochmuller H. Scapuloperoneal syndrome type Kaeser and a wide phenotypic spectrum of adult-onset, dominant myopathies are associated with the desmin mutation R350P. Brain. 2007; 130:1485-1496.
51. Capetanaki Y, Milner DJ, Weitzer G. Desmin in muscle formation and maintenance: knockouts and consequences. Cell Struct Funct. 1997; 22:103-116.
52. Babai F, Musevi-Aghdam J, Schurch W, Royal A, Gabbiani G. Coexpression of alpha-sarcomeric actin, alpha-smooth muscle actin and desmin during myogenesis in rat and mouse embryos I. Skeletal muscle. Differentiation. 1990; 44:132-142.
53. Wu Y, Zhang X, Salmon M, Lin X, Zehner ZE. TGFbeta1 regulation of vimentin gene expression during differentiation of the C2C12 skeletal myogenic cell line requires Smads, AP-1 and Sp1 family members. Biochim Biophys Acta. 2007; 1773:427-439.
54. Lindqvist J, Torvaldson E, Gullmets J, Karvonen H, Nagy A, Taimen P, Eriksson JE. Nestin contributes to skeletal muscle homeostasis and regeneration. J Cell Sci. 2017; 130:2833-2842.
55. Michalczyk K, Ziman M. Nestin structure and predicted function in cellular cytoskeletal organisation. Histol Histopathol. 2005; 20:665-671.
56. Collins K, Sellers J, Matsudaira P. Myosin I: a new insight into the mechanism and cellular significance of actin-based motility. Advances in biophysics. 1991; 27:221-226.
57. Qu G, Yan H, Strauch AR. Actin isoform utilization during differentiation and remodeling of BC3H1 myogenic cells. J Cell Biochem. 1997; 67:514-527.
58. Lee J, Robinson ME, Ma N, *et al*. IFITM3 functions as a PIP3 scaffold to amplify PI3K signalling in B cells. Nature. 2020; 588:491-497.
59. Chu PY, Huang WC, Tung SL, Tsai CY, Chen CJ, Liu YC, Lee CW, Lin YH, Lin HY, Chen CY, Yeh CT, Lin KH, Chi HC. IFITM3 promotes malignant progression, cancer stemness and chemoresistance of gastric cancer by targeting MET/AKT/FOXO3/c-MYC axis. Cell & bioscience. 2022; 12:124.
60. Min JQ, Feng Q, Liao WJ, Liang YM, Gong CW, Li EL, He WF, Yuan RF, Wu LQ. IFITM3 promotes hepatocellular carcinoma invasion and metastasis by regulating MMP9 through p38/MAPK signaling. Febs Open Bio. 2018; 8:1299-1311.

Received April 10, 2023; Revised June 15, 2023; Accepted August 15, 2023.

**Address correspondence to:*
Yanqin Lu and Jinxiang Han, Shandong First Medical University & Shandong Academy of Medical Sciences, No. 6699 Qingdao Road, Ji'nan, 250117, China.
E-mail: yqlu@sdfmu.edu.cn; jxhan@sdfmu.edu.cn

Released online in J-STAGE as advance publication August 18, 2023.